Computations of free-surface flows in porous media composed of swelling objects

Kodai Nagano[1,*], Daisuke Toriu[2], Satoru Ushijima[2]

[1]Civil Engineering, Graduate School of Engineering, Kyoto University, Japan
[2]ACCMS, Kyoto University, Japan

[*]nagano.koudai.33a@st.kyoto-u.ac.jp

Abstract.

To investigate the influences of swelling objects on free-surface flows, computations of dam-break flows in porous media composed of swelling objects were conducted in this study. Before the investigation of the swelling objects, the numerical method was applied to lock-exchange flows in porous media composed of non-swelling objects to check its applicability. As a result, the calculated front positions were in good agreement with the results reported by Ozan et al. After that, computations were conducted on dam-break flows in porous media composed of swelling objects considering different swelling rates. To clarify the difference in their flow patterns, the water surface heights were compared. The results showed that the dam-break flow was stopped by swelled objects and the water was trapped when the swelling rate is large.

Keywords: swelling object, porous media, free-surface flow, incompressible fluid

1. Introduction

Behaviors of swelling objects (e.g., superabsorbent polymers) in the fluid were experimentally and numerically investigated in previous studies [1]. On the other hand, it is also important to investigate the influences of swelling objects on flow patterns. For example, the changes of flow paths caused by swelling of objects are non-negligible to evaluate the water-absorbing performance of porous media composed of superabsorbent polymers, since the water flow can be stopped and trapped by the swelled objects when their swelling rate is large.

To investigate the influence of swelling objects, computations of dam-break flows in porous media composed of swelling objects are conducted considering the difference of swelling rates. Through the numerical experiments, the relationship between the swelling rates and the flow patterns are discussed.

2. Numerical method

The governing equations for isothermal incompressible gas and liquid based on the phase-averaged model are given by the following incompressible condition, conservation equation

of mass and momentum equations:

$$\frac{\partial u_j}{\partial x_j} = 0 \tag{1}$$

$$\frac{\partial \rho}{\partial t} + \frac{\partial (\rho u_j)}{\partial x_j} = 0 \tag{2}$$

$$\frac{\partial u_i}{\partial t} + \frac{\partial (u_i u_j)}{\partial x_j} = -\frac{1}{\rho}\frac{\partial p}{\partial x_i} + \frac{1}{\rho}\frac{\partial}{\partial x_j}\left(\mu \frac{\partial u_i}{\partial x_j}\right) - g\delta_{i2} \tag{3}$$

where t is the time, x_i $(i = 1, 2)$ is the component of the Cartesian coordinate system in which x_2 is the vertical component, u_i is the mass-averaged velocity component, g is the gravitational acceleration and δ_{ij} is Kronecker delta. The pressure p, the fluid density ρ and the coefficient of viscosity μ are volume-averaged variables. Equations (1), (2) and (3) are discretized by the finite volume method on the collocated grid system with the SMAC method [2]. For the convection terms, the 3rd-order TVD method is applied [3]. In addition, C-HSMAC method [2] is applied for the calculation of pressure to satisfy the incompressible condition.

The computational cell is treated as a solid cell when its cell center is included in the object region. In the solid cell, velocities at the cell center are defined as: $u_i = 0$. On the boundaries of the solid cell which face to fluid cells, non-slip conditions are imposed.

3. Results and discussions

3.1. Lock-exchange flow in porous media composed of non-swelling objects

Computations are conducted on lock-exchange flows in porous media composed of non-swelling square objects to check the applicability of the numerical method. The time history of front positions is compared with the results reported by Ozan et al. [4]. The height of the calculation area is H and the width is $12H$ as shown in Fig. 1, where H is 1.0. Non-slip conditions are imposed on all boundaries of the calculation area. The left half of the area is filled with the dense fluid whose density is ρ_w and coefficient of viscosity is μ_w. The right half is filled with the less dense fluid whose density is ρ_a and coefficient of viscosity is μ_a. In this numerical experiment, $\rho_w, \rho_a, \mu_w, \mu_a$ are 1001, 1000, 0.6667, 0.6673, respectively. In addition, the gravitational acceleration g is 10.0. Nondimensional variables are used for the numerical experiments of lock-exchange flows.

The square objects in the calculation area are arranged in a regular staggered pattern whose spacing length s is defined as shown in Fig. 1. The volume fraction of solids ϕ_s in the calculation area is given by $\phi_s = 2D^2/s^2$ where D is the side length of the square object and D is 1.0. Three different values of ϕ_s are considered in the computations, namely $\phi_s = 0.0125,\ 0.050,\ 0.120$ corresponding to $s = 0.4048,\ 0.2024,\ 0.1306$, respectively. The number of computational cells is 2400×200.

Figure 2 shows the time history of front position x_f of the dense fluid normalized by H. The interface of the fluids is defined as $\phi_\rho = 0.01$, where ϕ_ρ is normalized density given by $\phi_\rho = (\rho - \rho_a)/(\rho_w - \rho_a)$. The reference time t_0 is given by $t_0 = \sqrt{H\rho_w/g(\rho_w - \rho_a)}$. From Fig. 2, the results in this study are in good agreement with the results reported by Ozan et al. [4].

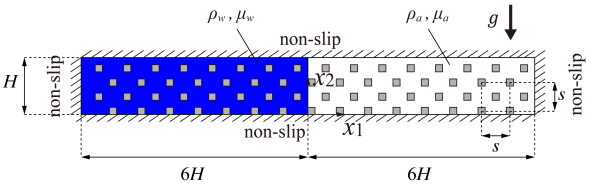

Figure 1: Calculation area containing objects

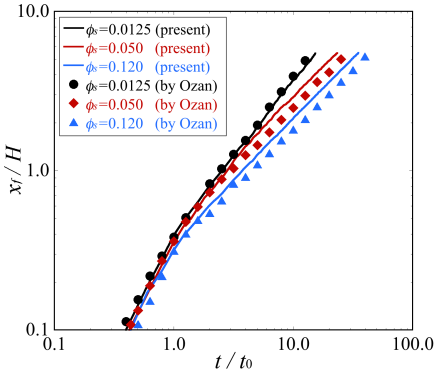

Figure 2: Time history of front positions (with results by Ozan et al. [4])

3.2. Dam-break flow in porous media composed of swelling objects

Four cases of dam-break flows are considered to investigate the influence of swelling objects on free-surface flows. In Case 1, no object is set in the calculation area which is the same condition as experiments by Koshizuka et al. [5]. As a result, the time history of front positions is in good agreement with the experimental results by Koshizuka et al. [5].

In Case 2, the calculation area contains non-swelling circular objects. While, in Cases 3 and 4, the calculation area contains swelling circular objects whose swelling rates v_r are v_0 and $4v_0$, respectively, where v_0 is 1.46×10^{-2} [m/s]. The radius r of objects becomes larger in time with the swelling rate which means $r = r_0 + v_r t$, where $r_0 = 1.46\times10^{-2}$ [m] is the radius at the initial state ($t = 0$ [s]). In the computations, the swelling is independent of the flows and continues until objects touch each other and the bottom boundary. The length of the width and height of the calculation area is L as shown in Fig. 3, where L is 0.584 [m]. Non-slip conditions are imposed on all boundaries of the calculation area. The width of the water column is $L/4$ and the height of that is $L/2$ in the initial state. The density and the coefficient of viscosity ρ_w, ρ_a, μ_w, μ_a are 0.9966×10^3 [kg/m^3], 1.763 [kg/m^3], 8.544×10^{-4} [Pa · s], 1.862×10^{-5} [Pa · s], respectively, where subscripts w and a represent water and air phases. The gravitational acceleration g is 9.81 [m/s^2].

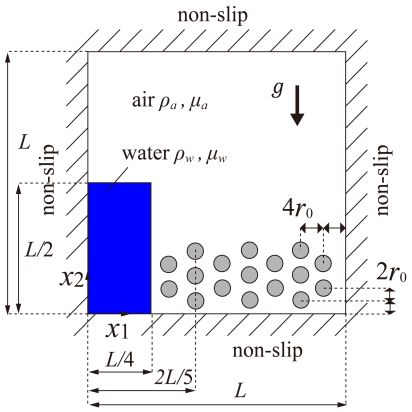

Figure 3: Calculation area and initial condition of water column

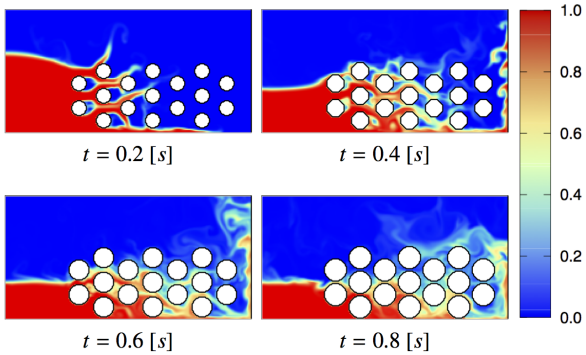

Figure 4: Distributions of ϕ_ρ in Case3

Figure 4 shows the distributions of ϕ_ρ in Case 3. From the figures, objects become larger in time and they disturb dam-break flow. Flow paths become narrower with the swelling of objects. Figure 5 shows the distributions of ϕ_ρ at $t = 0.25$ [s] in each case. The figures in Cases 2, 3 and 4 show that the dam-break flows are disturbed by the objects. Especially in Case 4, the flow is stopped by the swelled objects and the water is trapped in the left side of them. Figure 6 shows the time history of water surface heights H_L at the left end of the calculation area and the length $6r$ normalized by $L/2$, where $6r$ represents the summation of the thickness of solid objects on the vertical plane at $x_1 = 2L/5$. The reference time $t_1 = 0.25$ [s] which is the time swelling stops in Case 4. In Case 1, the result is plotted until $t = 4t_1$ since the front position has already reached the right wall. In Cases 1, 2 and 3, the water surface heights become smaller in time. On the other hand, in Case 4 the normalized water surface height stays around 0.6 which is the total height of objects at $x_1 = 2L/5$ after swelling stops. This shows the water is trapped by swelled objects in Case 4.

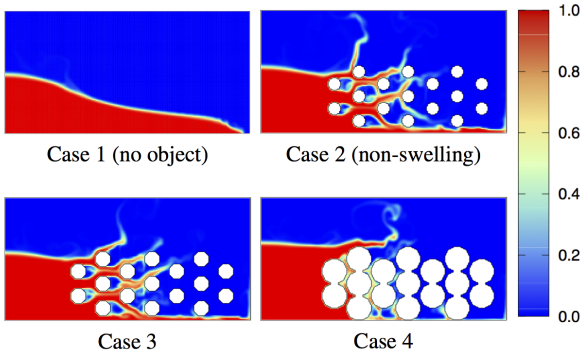

Figure 5: Distributions of ϕ_ρ at $t = 0.25$ [s]

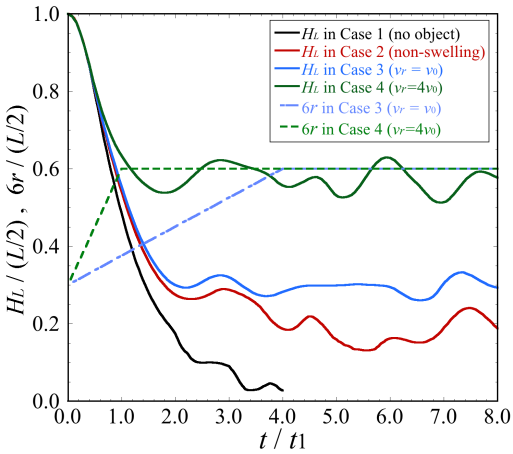

Figure 6: Time history of H_L and $6r$ normalized by $L/2$

References

[1] T. Sweijen, B. Chareyre, S.M. Hassanizadeh, N.K. Karadimitriou: Grain-scale modelling of swelling granular materials; application to super absorbent polymers, *Powder Technol.*, volume:318 (2017), 411–422.

[2] S. Ushijima, H. Tanaka, D. Toriu: Validity of Pressure-Velocity Correction Algorithm (C-HSMAC method) for Incompressible Fluids with Passive Scalar Convection, *J. Adv. Simul. Sci. Eng* volume:6 (2019), 260–272.

[3] A. Harten: High Resolution Schemes for Hyperbolic Conservation Laws, *J. Comput. Phys.* volume:49 (1983), 357–393.

[4] A.Y. Ozan, G. Constantinescu, A.J. Hogg: Lock-exchange gravity currents propagating in a channel containing an array of obstacles, *J. Fluid Mech.*, volume:765 (2015), 544–575.

[5] S. Koshizuka, Y. Oka: Moving-Particle Semi-Implicit Method for Fragmentation of Incompressible Fluid, *Nucl. Sci. Eng*, volume:123 (1996), 421–434.